 doi:10.20944/preprints202103.0259.v1

Article

Effect of Vanadium on Structural and Optical Properties of Borate Glasses Containing Er^{3+} and Silver Nanoparticles.

Nur Adyani Zaini [1], Syafawati Nadiah Mohamed [2] and Zakiah Mohamed [2, *]

[1] Faculty of Applied Sciences, Universiti Teknologi MARA, UiTM, Shah Alam 40450, Selangor, Malaysia; adyanizaini@gmail.com

[2] Faculty of Applied Sciences, Universiti Teknologi MARA, UiTM, Shah Alam 40450, Selangor, Malaysia; syafawati@uitm.edu.my; zakiah626@uitm.edu.my

* Correspondence: zakiah626@uitm.edu.my; Tel.: +60183708386

Abstract: Glass samples (59.5 – x) B_2O_3 – 20Na_2O – 20CaO – xV_2O_5 – Er_2O_3 – 0.5AgCl (x = 0 – 2.5 mol%) were prepared using melt – quenching method to investigate the structural and optical properties of the glass. The structural of the glass were characterized by using XRD, TEM and FTIR, meanwhile the optical properties were characterized by UV – VIS absorption. The XRD patterns confirmed the amorphous nature of the prepared glass samples. FTIR confirmed the presence of VO_4, VO_5, BO_3, and BO_4 vibration, and this result showed NBO increased with increasing vanadium concentration. The UV – Vis – NIR spectra exhibits six absorption band centered at 490, 520, 540, 660, 800, and 980 nm. The optical band gap (E_{opt}), Urbach energy and refractive index shown decrease, increase and increase, respectively. The Judd – Ofelt intensity parameter reveal the trends was $\Omega_2 > \Omega_4 > \Omega_6$. There are three emission bands at 516 nm, 580 nm, and 673 nm which are represented by $^2H_{11/2}$ – $^4I_{15/2}$, $^4S_{3/2}$ – $^4I_{15/2}$, and $^4F_{15/2}$ – $^4I_{15/2}$, respectively under 800 nm excitation was obtained.

Keywords: Borate glasses; silver nanoparticle, UV – VIS – NIR; Judd – Ofelt theory; Photoluminescence

1. Introduction

A Boron base oxide has unique properties. The properties are high transparency, low melting point, good rare-earth ion solubility, low crystallization ability, high dielectric constant, high thermal ability, cheap cost, different coordinate number, easy preparation in bulk form, low – cost preparation, large phonon energy (~1300 – 1500 cm^{-1}), resist vibration, lower viscosity, low refractive index and excellent forming ability due to small heat fusion, lower cation size, and higher bond strength.[1, 2, 3, 4, 5, 6]. All these properties make boron base glass suitable for noble optical devices [1, 2, 3, 4, 5, 6]. Boroxol is basically the form of pure boron B_2O_3. However, there are some transformation of BO_3 (Non – Bridge Oxide) units into BO_4 (Bridge Oxide) with some weakly attached BO_3 triangles, BO_4 tetrahedrons, some BO_4^- units without the formation of NBO [7, 8] and a variety of super-structural units such as tri–, penta–, tetra–, di–, pyro– and ortho – borate if B_2O_3 was added with some modifier oxides. For example, when alkali or alkaline – earth metal oxide into the glass as a modifier elastic, boron glass shows borate anomaly[5]. The borate anomaly was explained by considering the transformation of three – to four-fold coordinated boron during the initial addition of modifier oxide, but high content of modifier will create non – bridge oxygen (NBO) [6].

On the other hand, the incorporation of two dissimilar former glass produces a phenomenon called a mixed glass former effect (MGFE) [7]. When vanadium (V_2O_5) was introduced into boron (B_2O_3) it is formed from borovanadate glass consisting of mixed network former. Vanadium is a conditional that can form glass with the addition of other components under the conventional quenching method. However, the role of vanadium is depending on concentration [5], where at high concentration can be considered as

 doi:10.20944/preprints202103.0259.v1

former glass while low concentration vanadium can be considered as modifier [7, 10]. In this mixed glass former effect composition has attracted interest because of their interesting structural and physical properties.

Besides, vanadium is one of the approaches to overcome clustering due to high concentration of erbium. Normally, to achieve strong emission ,high concentration of erbium is required [9], but when high doping level of erbium may cause clustering, which leads to luminescence quenching and large non-radiative losses[10]. Thus, there are several approaches to overcome this issue which are heat-treated to produce glass – ceramic, introduce metallic nanoparticle [9] and co – doped with various rare – earth ions or transition metal [13, 14]. Previous reports confirmed that the emission intensity is stronger for system erbium ion – doped glasses co – doped with other rare earth such as Tm^{3+}, Nd^{3+}, and Yb^{3+} compared with single erbium ion doped glass. Thus, the emission could be achieved through the introduction of both co – doping rare – earth with transition and metallic nanoparticles (NPS).

The participation of vanadium ion in radiative transitions within the glass network has been studying in the emission spectra of $40Na_2O - 54SiO_2 - (5 - x)\ ZrO_2 - Ho_2O_3 - xV_2O_5$ [11] and $40Na_2O - 54SiO_2 - (5 - x)\ ZrO_2 - Sm_2O_3 - xV_2O_5$ glasses [13]. An additional band appeared at 636 nm and 1095 nm due to the transition $^2B_2 \rightarrow {}^2B_g$ and $^2B_2 \rightarrow {}^2E_g$ when V_2O_5 was added. The addition of V_2O_5 in a host matrix has been suggested to improve luminescence efficiency and lower phonon energies. Hence, the concentration V_2O_5 was believed to be the local environment of rare-earth ions in the oxides glass not only dependent on the composition of the host matrix. Thus, the concentration of vanadium may contribute to different crystal field strength. There are several studies regarding the emission properties of V_2O_5 doped rare – earth glass, but further research is required to facilitate a better understanding of the role V_2O_5 in modifying of glasses.

In this paper, the effect of vanadium on the structural and optical properties in the $(59.5 - x)\ B_2O_3 - 20Na_2O - 20CaO - xV_2O_5 - Er_2O_3 - 0.5AgCl$ (x = 0, 0.5, 1.0, 1.5, 2.0 and 2.5 mol%) glasses were studied. The structural properties were studied by X – ray diffraction (XRD), the fourier transformed infrared (FTIR) and transmission electron microscopy (TEM). The Uv – Vis spectrometer and photoluminescence spectrometer (pL) were used to study the absorption and luminesce spectra of the glass samples. Judd – Ofelt intensity parameter were calculated based on absorption spectra. Additionally, the radiative properties including effective band width, radiative transition probability, radiative lifetime and branching ratio were measured and analyzed.

2. Materials and Methods

2.1 Preparation of Glasses

Glass samples with the composition of $(59.5 - x)\ B_2O_3 - 20Na_2O - 20CaO - xV_2O_5 - Er_2O_3 - 0.5AgCl$ (x = 0, 0.5, 1.0, 1.5, 2.0 and 2.5 mol%) was prepared the by conventional melt quenching method. This composition enables the formation of transparent glass suitable for optical applications [7]. The appropriate amount of analytical grade commercial powder boron oxide (B_2O_3), sodium carbonate (Na_2CO_3), calcium carbonate ($CaCO_3$), vanadium oxide (V_2O_5), erbium oxide (Er_2O_3), silver chloride (AgCl) (purity ≥ 99 %) was mixed and weighed homogeneously. At 1200 °C, the homogeneous mixture melted in alumina crucibles for one hour. Then, the samples were quenched into a stainless plate and mould. The samples were annealed at 300°C for three hours in another furnace. After three hours, the furnace will automatically stop the process and reduced the temperature by itself gradually until room temperature. This process allowed the samples to cool down. The glass samples were polished using sandpapers to get a parallel opposite surface with thickness approximately five mm for optical absorption and photoluminescent spectroscopy. The glass samples were powderized for X-ray diffraction (XRD), transmission electron microscopy (TEM) and infrared (IR) absorption characterization.

Preprints (www.preprints.org) | NOT PEER-REVIEWED | Posted: 9 March 2021 doi:10.20944/preprints202103.0259.v1

2.2 Characterization of Glasses

The glasses were examined by X – Ray Diffraction analysis using X'Pert Pro Panalytical diffrection to confirm the amorphous present in the samples. The formation crystalline plane in silver nanoparticles confirmed using Transmission electron microscopic (TEM). A small amount of powder samples dispersed into acetone liquid using ultrasonic bath. The solution was placed onto copper grid and allowed to dry before it was ready to characterization. Archimedes principle used to determine the density of the glass samples. The immersion medium was toluene [14, 15] at room temperature. The density of the glass samples was calculated standard relation 1:

$$\rho = \frac{w_a}{w_a - w_b} \times \rho_o \quad (1)$$

Where w_a and w_b are the glass samples weight in the air and the toluene respectively while ρ and ρ_o are a density of the glass samples and density of toluene (0.8669 gcm^{-3}) [16, 17]. The values of molar volume (V_a) were calculated using equation 2;

$$V_a = \frac{M_V}{\rho} \quad (2)$$

Where M_v is the molar mass of the samples [17].

A Perkin Elmer UV-Vis-NIR Spectrophotometer in the range 200 nm – 1000 nm was used to record the optical absorption spectra at room temperature. The functional group within the range 400 cm^{-1} – 1600 cm^{-1} with 4 cm^{-1} at room temperature were investigated by the IR absorption spectra of the glass samples. The Perkin Elmer model Spectrum One FTIR spectrometer was used to record the glass powder sample's IR absorption spectra. The powder glass samples were mixed with KBr at a fixed ratio 1:80. The mixed powder was pressed into pallet through hand press. The visible up-conversion emission measurement was carried out in the wavelength region 200 – 900 nm at room temperature by Perkin LS-55 luminesce spectrometer in which a pulsed Xenon lamp operates as source of excitation.

3. Results

3.1 XRD, TEM and Physical Properties

The XRD patterns of (59.5 – x) B_2O_3 – 20Na_2O – 20CaO – xV_2O_5 – Er_2O_3 – 0.5AgCl (x = 0, 0.5, 1.0, 1.5, 2.0 and 2.5 mol%) glass samples are shown in Figure 1. The figure 1 revealed the presences of two broad humps at approximately 20° – 40° and 40° – 60°for all the samples. These two broad humps phase separation where the samples consisted of two mid – range phases. The present of broad humps indicated the amorphous nature of all the glass samples.

Preprints (www.preprints.org) | NOT PEER-REVIEWED | Posted: 9 March 2021 doi:10.20944/preprints202103.0259.v1

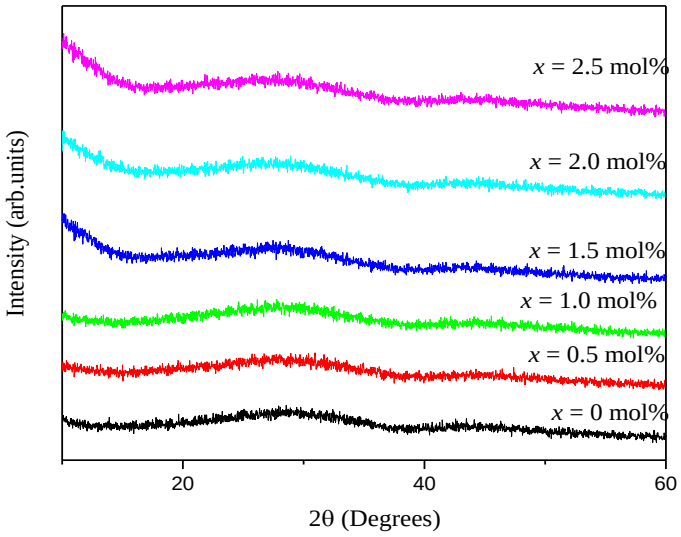

Figure 1. This is a figure of XRD patterns of (59.5 – x) B_2O_3 – 20Na_2O – 20CaO – xV_2O_5 – Er_2O_3 –0.5AgCl (x = 0, 0.5, 1.0, 1.5, 2.0 and 2.5 mol%).

Figure 2 shows one of representative TEM image of glass for x = 1.0 mol%. The average size of the black spherical spot in glass sample (x = 1.0 mol%) is five nm confirmed by the TEM image. Therefore, the black spherical spot in the figure 2(a) can be conclude as silver nanoparticle. In the figure 2(a) clearly shows some black spherical spots and homogeneous distribute of silver nanoparticles in the glass samples.

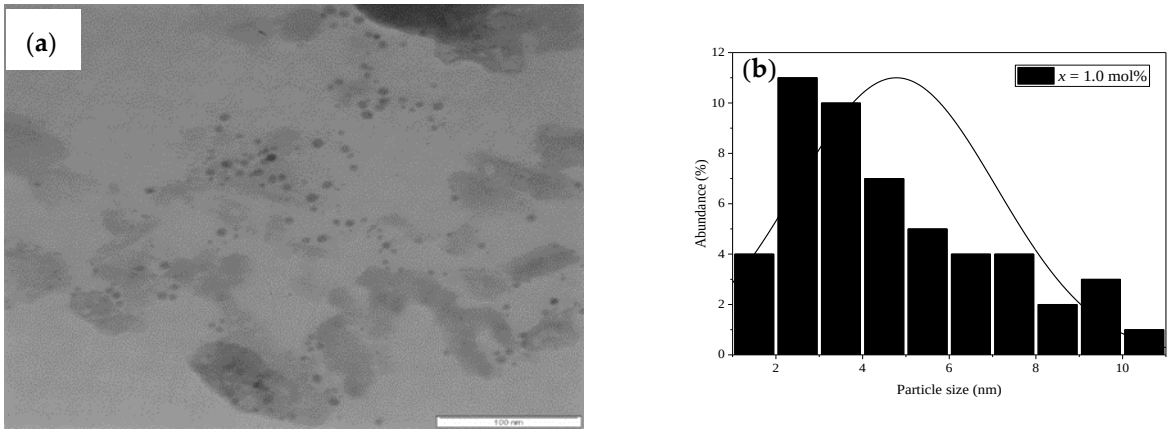

Figure 2. This are the figures of (**a**) TEM image of glass 1.0 mol% of vanadium contents; (**b**) histogram of the size distribution of the metallic silver NPs.

Table 1 provides the values of density, molar volume, and refractive index, for (59.5 – x) B_2O_3 – 20Na_2O – 20CaO – xV_2O_5 – Er_2O_3 – 0.5AgCl (x = 0, 0.5, 1.0, 1.5, 2.0 and 2.5 mol%) glass samples. Figure 3 showed the variation in density and molar volume with concentration of vanadium for glass samples. The density of the samples showed a non-linear increase while the molar volume of the samples increased monotonically in the figure 3. These sample patterns are good agreement when compared with the previous report [5]. The density value is between 2.494 gcm^{-3} and 2.521 gcm^{-3} meanwhile, the molar volume in the range 27.898 cm^3mol^{-1} to 28.709 cm^3mol^{-1} with addition of V_2O_5 into the

Preprints (www.preprints.org) | NOT PEER-REVIEWED | Posted: 9 March 2021 doi:10.20944/preprints202103.0259.v1

glass samples. These density values are smaller than (60 – x) B_2O_3 – 20Na_2O – 20CaO – xV_2O_5 (2.537 – 2.550 gcm^{-3}), while the molar volume is bigger than (60 – x) B_2O_3 – 20Na_2O – 20CaO – xV_2O_5 (25.77 – 26.73 cm^3mol^{-1}) [5].

Table 1. This is a table for the values of density (ρ) and molar volume (V_a) for (59.5 – x) B_2O_3 – 20Na_2O – 20CaO – xV_2O_5 – Er_2O_3 – 0.5AgCl (x = 0, 0.5, 1.0, 1.5, 2.0 and 2.5 mol%).

Samples (mol%)	Density (gcm^{-3})	Molar volume(cm^3mol^{-1})
x = 0	2.494	27.898
x = 0.5	2.507	27.960
x = 1.0	2.504	28.233
x = 1.5	2.509	28.395
x = 2.0	2.520	28.492
x = 2.5	2.521	28.709

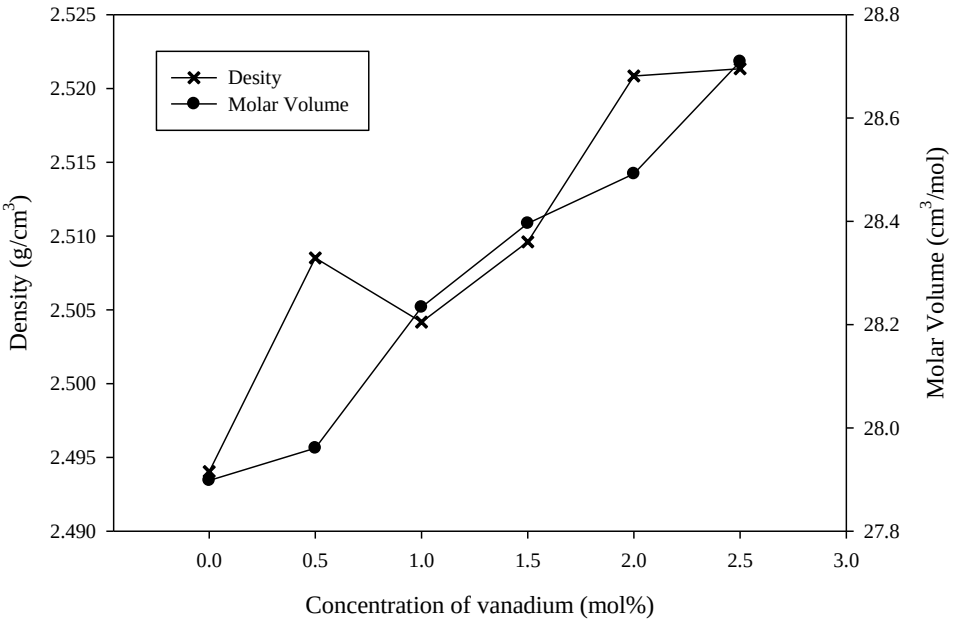

Figure 3. This is a figure of density (ρ) and molar volume (V_a) for (59.5 – x) B_2O_3 – 20Na_2O – 20CaO – xV_2O_5 – Er_2O_3 –0.5AgCl (x = 0, 0.5, 1.0, 1.5, 2.0 and 2.5 mol%).

The changes of molar mass and molar volume impact the density of the glass, and usually density and molar volume show contracting behavior. However, in the cases of study, the density and molar volume display same behavior, where both values increased with addition of vanadium. Others borate glass system also reported this behavior [5, 23].

The mass of B_2O_3 (M = 69.63 g mol^{-1}) is lighter compared with V_2O_5 (M = 181.88 g mol^{-1}). It can be concluded, the increase in density was due to replacement of lighter molecular (B_2O_3) with a heavier molecular (V_2O_5). Thus, the non – bridging oxygen increased with increasing V_2O_5 content.

The borate group consist of many B – O bonds and Vanadate groups contain various of V – O bonds. The bond length of BO_3 and BO_4 were 1.36Å and 1.47Å [19], respectively. While the previous classical molecular (MD) stimulation research reported that, the bond length of V^{5+} – O (1.81 – 1.92 Å) was slightly longer than the bond length of V^{4+} – O (1.74 – 1.85 Å) [20]. The bonds in borate group are shorter than bonds in vanadate group. Thus,

Preprints (www.preprints.org) | NOT PEER-REVIEWED | Posted: 9 March 2021 doi:10.20944/preprints202103.0259.v1

replacement of shorter B – O bond length with longer V – O bond length increase the molar volume and open the network structure of the glass samples.

3.2 IR Spectra

There are three mainly active infrared region for B_2O_3 – V_2O_5 [26, 27]. The group of bands that occur around 500-750 cm $^{-1}$ is due to bending of B – O – B linkages in the borate network. The bands lie between 800 – 1200 cm^{-1} is due to asymmetric vibration of BO_4 units. The third group is due to the asymmetric stretching relaxation of the B – O band of triagonal BO_3 units, and the band lies between 1200 – 1450 cm^{-1}. Other studies also reported the same results[21, 23].

IR absorption spectra for (59.5 – x) B_2O_3 – 20Na_2O – 20CaO – xV_2O_5 – Er_2O_3 –0.5AgCl (x = 0, 0.5, 1.0, 1.5, 2.0 and 2.5 mol%), were recorded in 400 - 1600 cm^{-1} region at room temperature is shown in the figure 4(a). Figure 4(b) show the deconvolution of spectrum at x = 1.0 mol% glass sample. Based on the figure 4, the vibrational modes of the borate network seen like to previous research [5]. The first region, the band at 1391 – 1407 cm^{-1} was attributed to the stretching vibration of NBO bond from metaborate, orthoborate and pyroborate of BO_3 unit. The band correlated to stretching vibration of B – O bonds in pentaborate, triborate, and tetraborate group of BO_4 units is located at about 927 – 1205 cm^{-1}. Mohamed et al [5] report that, region at 990 – 1024 cm^{-1} is overlapping with the vibration from VO_5 trigonal bipyramids unit of the V = O. They assumed that the band of vibration for isolated group B – O – V bridging bonds or V = O was located at 1000 cm^{-1}. The region from 511 – 536 cm^{-1} was assigned to the in – plane bending of B – O and the IR band at around 740 – 751 cm^{-1} was referred to the B – O – B bending vibration of BO_4 and BO_3 [5].

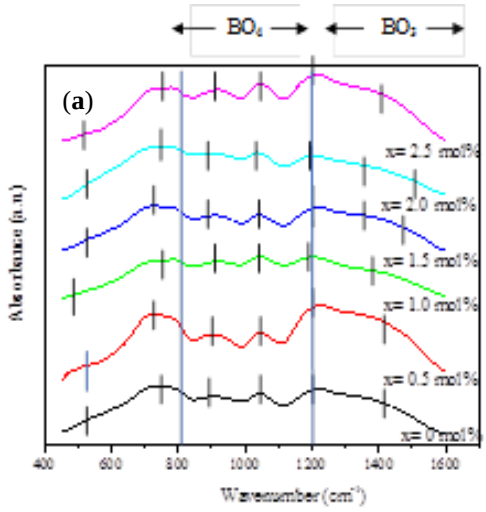

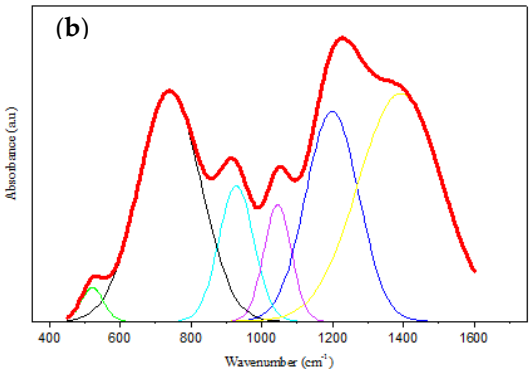

Preprints (www.preprints.org) | NOT PEER-REVIEWED | Posted: 9 March 2021 doi:10.20944/preprints202103.0259.v1

Figure 4. This are the figures FTIR results of the (**a**) (59.5 – *x*) B_2O_3 – 20Na_2O – 20CaO – *x*V_2O_5 – Er_2O_3 –0.5AgCl (*x* = 0, 0.5, 1.0, 1.5, 2.0 and 2.5 mol%), and (**b**) deconvolution of 59 B_2O_3 – 20Na_2O – 20CaO – 0.5V_2O_5 – Er_2O_3 –0.5AgCl.

To evaluate the impact of vanadium on borate structure, the relative area of BO_4 / V = O bands have been normalized by area of BO_4 at *x* = 0 mol%. Addition of 0.5 mol% vanadium increased the relative area of BO_3 functional group. However further addition of vanadium *x* > 0.5 mol% showed decreasing trend relative area BO_3 functional group. The addition of 0.5 mol% V_2O_5 contents, decreased the normalized plot of BO_4 / V = O but increased as increased the vanadium concentration into the glass samples. Increasing BO_4 / V = O and decreasing BO_3 indicates formation of NBO, whereas increasing BO_3 and decreasing in normalize BO_4 / V = O remarked increasing BO [19]. In this study, the NBO increased when the concentration of the vanadium *x* > 1.0 mol%.

3.3 UV-VIS Properties

Figure 5 shows the absorption spectra for (59.5 – *x*) B_2O_3 – 20Na_2O – 20CaO – *x*V_2O_5 – Er_2O_3 – 0.5AgCl (x = 0, 0.5, 1.0, 1.5, 2.0 and 2.5 mol%). The absorption spectra contain six bands placed at 490, 520, 540, 660, 800, and 980 nm. Comparing with other findings, all the peaks are referring the erbium absorption from the ground state $^4I_{15/2}$ to the excited states $^4F_{7/2}$, $^2H_{11/2}$, $^4S_{3/2}$, $^4F_{9/2}$, $^4I_{9/2}$, and $^4I_{11/2}$ respectively [24]. In comparison of peaks, the transition $^4I_{15/2} \rightarrow {}^2H_{11/2}$ with wavelength 520 nm has the highest peak. There are no new band was observed with addition of vanadium in the samples. It can be concluded, the bands due to vanadyl ion was not observed in recorded spectra or maybe overlap with erbium band. This is because to the dominance of erbium ion band intensity. The erbium ion intensity dominance, the SPR band contributed by silver nanoparticles also is not observed. There are many previous studies reported that the SPR band is expected to be around 400 – 500 nm [25, 26]. The SPR frequency is depending on the refractive index (n ~2 for borate glass) and dielectric function of silver [27].

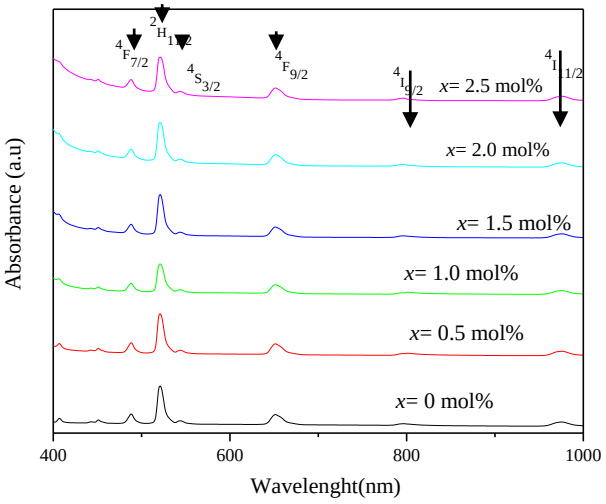

Figure 5. This is a figure for Uv – Vis – NIR absorption spectra of (59.5 – *x*) B_2O_3 – 20Na_2O – 20CaO – *x*V_2O_5 – Er_2O_3 –0.5AgCl (*x* = 0, 0.5, 1.0, 1.5, 2.0 and 2.5 mol%).

3.4 Optical Properties

The optical properties of amorphous material can be studied mainly regarding electronic band structure and optical transition. An electron in the valence band interacts

Preprints (www.preprints.org) | NOT PEER-REVIEWED | Posted: 9 March 2021 doi:10.20944/preprints202103.0259.v1

with an electromagnetic wave, it has enough energy to rise across the bandgap to the conduction band. The energy required to cross the band gap closely related to the optical energy bandgap (E_{opt}).

The optical absorption edge is used to investigate the electronic transition during absorption. The absorption coefficient (α) can be calculated at various wavelength using the Beer-Lambert Law [5]

$$I = I0e^{\alpha t} \tag{3}$$

Where I_0, it is the incident and transmitted photon intensities. The samples thickness is t. By drawing a Tauc plot (figure 6) according Davis and Mott relation with α as follow[5]:

$$\alpha(\omega) = \frac{A\,(h\nu - E_{opt})^n}{h\nu} \tag{4}$$

Where h is plank constant v is the photon frequency, A is a constant, and n is a constant determining the types of transition. The n constant has different values of 2, 3, 1/2, or 1/3, which referring to indirect allowed, indirect forbidden, direct allowed, and direct forbidden transition, respectively [28]. The value of n for the oxide glass is 2 [5]. In this study, the graph $h\nu$ against $(\alpha h\nu)^2$ has been plotted (Figure 6) and used to measure the optical band gap. The optical band gap is the intersection of the straight line of the curve at x-axis when the $(\alpha h\nu)^2 = 0$ [24]

Preprints (www.preprints.org) | NOT PEER-REVIEWED | Posted: 9 March 2021 doi:10.20944/preprints202103.0259.v1

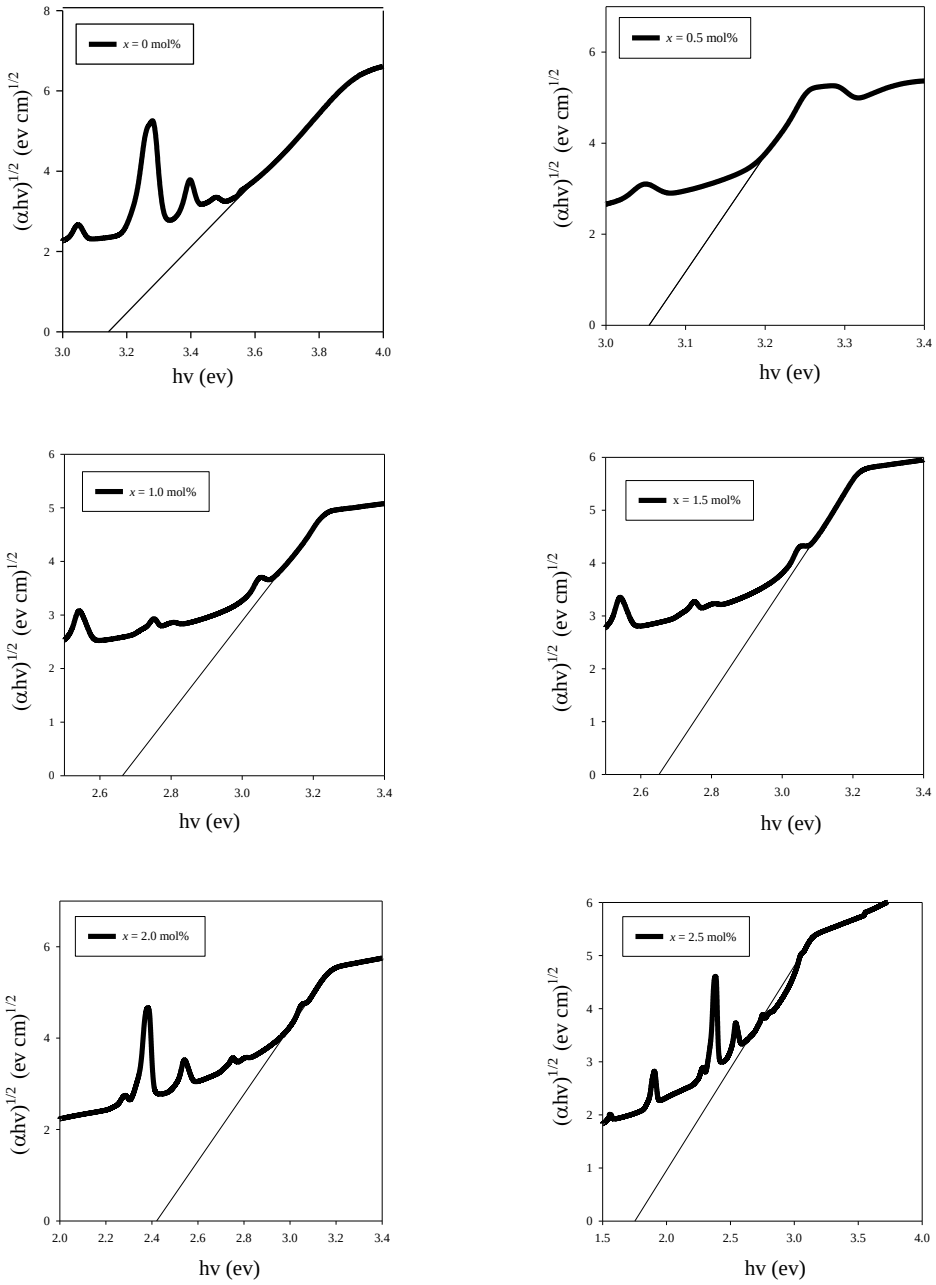

Figure 6. This is a figure for straight line of the curve at x-axis when the $(\alpha hv)^{1/2} = 0$.

The changes of band gap energy can be explained by the increase of decrease of disorder in the material. Using Urbach's equation, the disorder can be calculated [5].

$$\alpha(v) = Cexp\left(\frac{hv}{Eu}\right) \quad (5)$$

Where α is a constant, and Eu is the urbach energy. The graph of ln (α) versus hv were plotted in Figure 7. The reciprocal of the slope of the linear to the curve referring to the urbach energy [5]. Urbach energy depended on several factors: temperature, average photon energy, induced disorder, static disorder, thermal vibration in the lattice, and strong ionic bond.

Preprints (www.preprints.org) | NOT PEER-REVIEWED | Posted: 9 March 2021 doi:10.20944/preprints202103.0259.v1

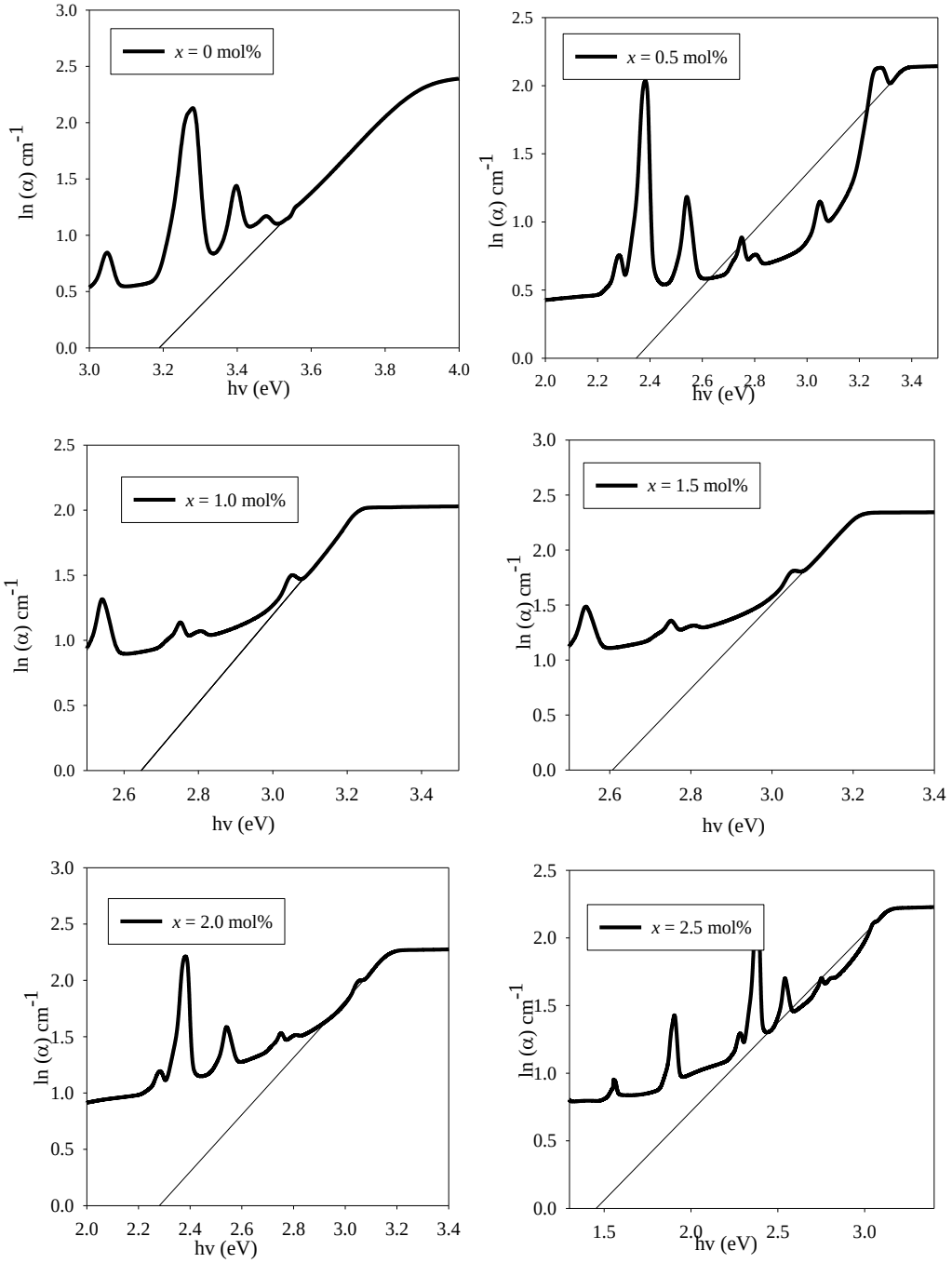

Figure 7. This is a figure of Urbach energy.

Table 2 shows the values of indirect energy band gap, Urbach energy, and refractive index of for all the samples. The energy band gap (E_{opt}) values in the range 3.143024 – 1.752474 eV. E_{opt} decreased with increased vanadium concentration. The variation in E_{opt} and n against V_2O_5 concentration show contrasting behavior in figure 8, whereby n increased with increased vanadium concentration. This behavior has been showed for previous research [5]. The n values that lie in the range of 2.359592 – 2.852138. In the studied glass samples, the reduction of band gap with increased V_2O_5 is due to structural evolution. For x < 1.0 mol%, the band gap decreases because increasing of NBO on borate triangular BO_3 at low concentration of vanadium. The creation of NBO opened the glass structure and the electron easier to excited compared with the case in BO because the electron was loosely bond in NBO. The band gap most likely constant for x =1.5 mol%

Preprints (www.preprints.org) | NOT PEER-REVIEWED | Posted: 9 March 2021 doi:10.20944/preprints202103.0259.v1

may be assumed to be due to the new role of V_2O_5 as former oxide. At low concentration, vanadium acts as network modifiers, while at high concentration, vanadium acts as network forming[11]. The structural revolution that happened with increasing vanadium concentration caused the contrasting behavior of n.

Table 2. This is a table for indirect optical energy band gap (E_{opt}), Urbach energy (E_U), and refractive index (n) of (59.5 – x) B_2O_3 – 20Na_2O – 20CaO – xV_2O_5 – Er_2O_3 – 0.5AgCl (x = 0, 0.5, 1.0, 1.5, 2.0 and 2.5 mol%).

x (mol%)	E_{opt} (eV)	E_U (eV)	n
0	3.143024	0.298338	2.359592
0.5	3.05428	0.481603	2.38261
1.0	2.663079	0.295727	2.494268
1.5	2.651355	0.261131	2.497905
2.0	2.420714	0.395163	2.497905
2.5	1.752474	0.762137	2.852138

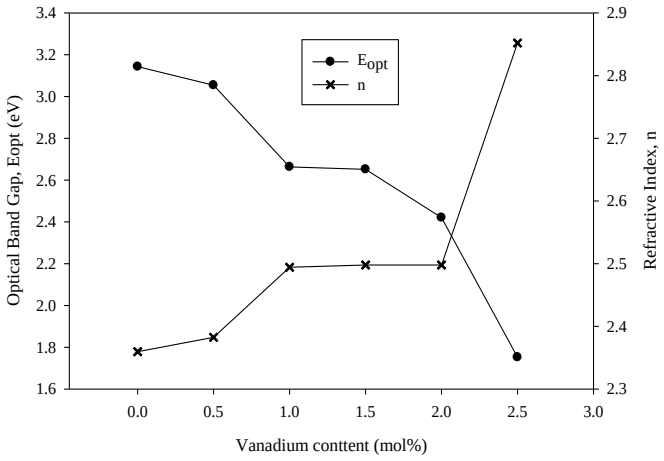

Figure 8. This is a figure for optical band gap (E_{opt}) and refractive index of (59.5 – x) B_2O_3 – 20Na_2O – 20CaO –xV_2O_5 – Er_2O_3 – 0.5AgCl (x = 0, 0.5, 1.0, 1.5, 2.0 and 2.5 mol%).

The E_U values of the glass increased sharply from 0.298338 - 0.481603 eV (x = 0 - 0.5 mol%), followed by a sharply decreased when 1.0 – 1.5 mol% of vanadium added into the glass samples. The E_U values gradual increased to 0.762137 (x = 2.5 mol%) with further increase in V_2O_5 content in Figure 9. The addition of vanadium x = 0.5 mol%, increase the Urbach energy value, which indicates the tendency of week bonds convert to defect increased. For x = 0.5 mol% the concentration of defect increased in the glass network with increased NBO. The Urbach energy value decreased for x = 1.0 and 1.5 mol%. This decrement suggests that, the degree of the disorder of the present glass decreased. However, for x > 1.5 mol% the Urbach energy increasing. The increase of Urbach energy impacted the decrease of energy band gap or decrease of Urbach energy, increase energy band gap.

Preprints (www.preprints.org) | NOT PEER-REVIEWED | Posted: 9 March 2021 doi:10.20944/preprints202103.0259.v1

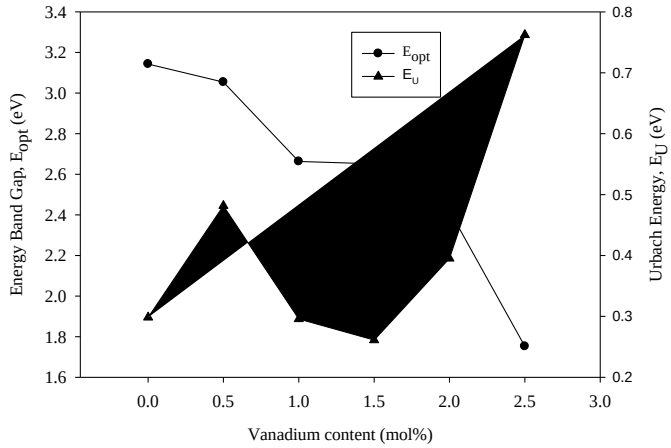

Figure 9. This is a figure for optical band gap (E_{opt}) and Urbach energy of (59.5 – *x*) B_2O_3 – 20Na_2O – 20CaO –*x*V_2O_5 – Er_2O_3 – 0.5AgCl (*x* = 0, 0.5, 1.0, 1.5, 2.0 and 2.5 mol%).

3.5 Judd – Ofelt Analysis

Judd-Ofelt theory provides the information of transition behavior between 4f – 4f electronic configuration and calculation of oscillation strength, intensity parameter (Ω_2, Ω_4, Ω_6), transition probabilities, and branching ration[29, 30]. The Judd – Ofelt theory is the best method to investigate and analyze the spectral properties of borate glass system containing rare earth ion (erbium ion). Absorption spectral data of all samples containing different concentration vanadium was used to calculate the Judd – Ofelt parameters. The precise integrated absorption cross section measurement over the range of wavelength and transition state of excitation is needed to analysis the Judd – Ofelt theory.

The area under the absorption band were used to determine the experimental oscillator strength. The experimental oscillator strength can be calculated via the relation:

$$f_{exp} = \frac{2303\ mc^2}{\pi e^2 N_0} \int \varepsilon_a(v)\, dv \tag{6}$$

$$= 4.32 \times 10^{-6} \int \varepsilon(v)\, dv \tag{7}$$

Where m is the electron mass, c is the velocity of light in vacuum, N_0 is the Avogadro's number, and is the $\varepsilon(v)$ molar extinction coefficient. The molar extinction coefficient obtained from the measured absorbance of the samples which was calculated from the Beer-Lambert law as follow:

$$\varepsilon_a(v) = \frac{\log_0 \frac{I_0}{I_t}}{c_{RE}\, t} \tag{8}$$

Preprints (www.preprints.org) | NOT PEER-REVIEWED | Posted: 9 March 2021 doi:10.20944/preprints202103.0259.v1

Where C_{RE} is the concentration of the rare earth ion (erbium) (mol/1000 cm^3), t is the thickness of the samples in cm and last but not least $\log_0 \frac{I_0}{I_t}$ is the calculated from absorbance at the wave-number υ (cm^{-1}).

The estimation of theoretical oscillator strength for a transition from the ground state to an excitation state of erbium ion within 4f configuration according to Judd-Ofelt theory as follow:

$$f_{cal} = \frac{8mc\upsilon\pi^2}{3h(2J+1)e^2}\frac{n^2+2}{9n}\left(e^2\sum_{\lambda=2,4,6}\Omega_\lambda| < aJ|U^{(\lambda)}|bJ' > |^2\right) \quad (9)$$

Where υ is the wavenumber of the transition in cm^{-1}, h is a plank constant, and J is the total angular momentum of the lowest state. The factor of $(n^2 + 2)/9n$ represents for the electric field correction of Lorentz, and n is the refractive index of the samples. Ω_λ is Judd – Ofelt intensity parameter where λ are 2,4, and 6. $||U^{(\lambda)}||$ represents the double-reduced square matrix elements of the unit tensor operator of rank λ = 2,4, and 6 are calculated using the intermediate coupling approximation method for transition lowest state to highest states. The reduce matrix elements $\Omega_\lambda| < aJ|U^{(\lambda)}|bJ' > |^2$ are calculated following Carnall *et al* [31].

To evaluate the accuracy of the Judd – Ofelt parameter, the quality of the fit was identified by the root-mean-square (rms) deviation relation:

$$rms = \left[\frac{\Sigma(f_{calc} - f_{exp})^2}{\xi - 3}\right]^{1/2} \quad (10)$$

Where ξ is three, the number of spectral bands analyzed. The values of rms indicates the quality of the fit between experimental oscillator strength and calculated oscillator strength. These values also show the accuracy of the Judd – Ofelt parameter.

Table 3 shows the rms and oscillator strength for calculated and experimental of all the glass samples. Indirect data on the symmetry and bonding of rare earth ions within the matrix was provided by oscillator strength. The highest oscillator force attributed to the hyper-sensitive transition was shown by the transition band at $^4I_{15/2} \rightarrow {}^2H_{11/2}$. Such hyper-sensitive transitions are sensitive to changes in the local structure of the glass network. These hyper – sensitive transition comply with the $\Delta S = 0$, $|\Delta J| \leq 2$ and $|\Delta L| \leq 2$ selection rules and reflects the interaction strength of erbium ions in the local network with host glass. In the present glass samples, with the increase in vanadium content, increases in the oscillator strength of hyper – sensitive transition. These changes reveal strong covalency with the presence of lower symmetry around erbium ions. These values are found have highest oscillator strength comparing with phosphate glass[14, 32], boro – aluminosilicate glass[10] and tellurite glass[16, 26]. In addition, the values of rms are in the range $1 – 2 \times 10$. These very small rms value confirmed the accuracy of the data [33]. The rms values of all the glass samples are good agreement when compared with previous study [34].

Table 3. This is a table for calculated oscillator strength (f_{cal}, 10^{-6}), the experimental oscillator strength (f_{exp}, 10^{-6}) and rms of the erbium absorption transition from the ground state $^4I_{15/2}$ to the excited states.

Preprints (www.preprints.org) | NOT PEER-REVIEWED | Posted: 9 March 2021 doi:10.20944/preprints202103.0259.v1

Transition $^4I_{15/2}\rightarrow$	Glass samples											
	x = 0 mol%		x = 0.5 mol%		x = 1.0 mol%		x = 1.5 mol%		x = 2.0 mol%		x = 2.5 mol%	
	fcal	fexp	fcal	fexp	fcal	fexp	fcal	fexp	fcal	fexp	fcal	fexp
$^4I_{11/2}$	7.95	6.99	7.65	7.32	6.83	6.81	8.05	7.32	8.12	7.93	7.78	7.7
$^4I_{9/2}$	5.95	4.86	6.31	6.02	5.81	6.24	6.09	5.1	6.38	4.96	6.13	4.63
$^4F_{9/2}$	3.27	3.27	3.36	3.35	3.08	3.05	3.3	3.3	3.42	3.46	3.29	3.35
$^4S_{3/2}$	6.28	4.92	5.96	4.29	5.41	4.02	6.08	5.22	6.23	4.55	6.06	4.41
$^2H_{11/2}$	1.03	1.03	1.05	1.05	9.07	9.07	1.19	1.19	1.15	1.15	1.06	1.06
$^4F_{7/2}$	2.78	2.95	2.73	2.85	2.49	2.58	2.73	2.85	2.82	2.87	2.73	2.76
rms	1.53		1.22		1.03		1.10		1.33		2.86	

Table 4 shows the values of Judd – Ofelt intensity parameters ($\Omega_{2,\ 4,\ 6}$) and their spectroscopic properties (χ) along with trend of Judd – Oflet parameter for all the glass samples. The data of Judd – Ofelt parameter from previous reported literature will be utilized for comparison with current glass samples [34]. The composition of the glass determines the values of Judd – Ofelt parametes. The increasing in vanadium ions concentration from 0 to 1.0 mol% impact to decrease Ω_2 and Ω_6 values from 3.19×10^{-20} to 2.43×10^{-20} and 8.45×10^{-21} to 6.53×10^{-21}, respectively. In addition, it can be seen the trend of Ω_λ was found to $\Omega_2 > \Omega_4 > \Omega_6$ for all the glass prepared samples. The samples with Ω_2 and Ω_4 higher intensity parameters compared with Ω_6 can be regarded as the good glass host because have high luminescence intensity ratio and high covalent bond between erbium ion and local environment ligand [34, 35]. The values of Ω_2 and Ω_4 was smaller for borate glass containing erbium ion co – doped vanadium compared to borate glass containing erbium ion only [34]. The parameters Ω_2 and Ω_4 are highly sensitive to the rare earth ion's local environment symmetry. The small values of Ω_2 and Ω_4 indicates the lower asymmetric nature of the local environment around erbium ion exists in the glass system [37].

The Ω_6 contradict to the Ω_2 and Ω_4, where Ω_6 does not depend on the local structure [38] and normally the rigidity of the glass correlated to these parameter [34]. The glass without vanadium concentration (x = 0) more rigid compare to others glass samples (x = 0.5 – 2.5 mol%). Since the value of Ω_6 for glass without vanadium is bigger than other samples (with vanadium). The addition of vanadium ions concentration from 0 to 1.0 mol% leads to decrease Ω_6 values from 8.45×10^{-21} to 6.53×10^{-21}. This is because of NBO was created around the host matric. The creation of NBO causes high number of covalency and lead to produce high number of electron density of the ligand ions.

The values of Ω_4 and Ω_6 parameters was used to determine the spectroscopic quality factor (χ) [39]. The χ will define the efficiency of laser transition. Therefore, it can be used to predict the stimulated emission of the laser. The values of χ for all the glass samples in the range of 1.70781 – 1.95143. These values were bigger than erbium in tellurite glass system [24]. The bigger the value of χ reveals the higher efficiency of laser transition because according to [40] report that, the higher the value of χ, the more intense of the laser transition. In this study, the glass with 1.0 mol% of vanadium shows to be optically better compared to others glass samples.

Table 4. This is a table for Judd – Ofelt intensity parameter and spectroscopic quality factor for all prepared glass samples.

Glass samples	Ω_2 cm²	Ω_4 cm²	Ω_6 cm²	Trends of Ω_λ	$\chi = \Omega_4/\Omega_6$	Ref.
x = 0 mol%	3.19×10^{-20}	1.44×10^{-20}	8.45×10^{-21}	$\Omega_2 > \Omega_4 > \Omega_6$	1.70781	This work
x = 0.5 mol%	3.16×10^{-20}	1.51×10^{-20}	7.87×10^{-21}	$\Omega_2 > \Omega_4 > \Omega_6$	1.923875	This work
x = 1.0 mol%	2.43×10^{-20}	1.27×10^{-20}	6.53×10^{-21}	$\Omega_2 > \Omega_4 > \Omega_6$	1.95143	This work

Preprints (www.preprints.org) | NOT PEER-REVIEWED | Posted: 9 March 2021 doi:10.20944/preprints202103.0259.v1

x = 1.5 mol%	3.38×10^{-20}	1.32×10^{-20}	7.30×10^{-21}	$\Omega_2 > \Omega_4 > \Omega_6$	1.812267	This work
x = 2.0 mol%	3.21×10^{-20}	1.39×10^{-20}	7.49×10^{-21}	$\Omega_2 > \Omega_4 > \Omega_6$	1.849739	This work
x = 2.5 mol%	2.22×10^{-20}	1.00×10^{-20}	5.50×10^{-21}	$\Omega_2 > \Omega_4 > \Omega_6$	1.826248	This work
LiBEr5	4.39×10^{-20}	3.22×10^{-20}	5.50×10^{-21}	$\Omega_2 > \Omega_4 > \Omega_6$	5.85	[34]
BLNEr	3.35×10^{-20}	1.34×10^{-20}	7.89×10^{-21}	$\Omega_2 > \Omega_4 > \Omega_6$	1.69	[41]

The values of Ω_λ were used to calculate the radiative properties such as spontaneous emission rate (A_R), branching ratio (β_R), and lifetime of the radiative transition (τ_{rad}). The emission probabilities probabilities and called as Einstein coefficient for radiative transition A_R (aJ, bJ') of the different transition are calculated by,

$$A_R(aJ, bJ') = A_{ed} + A_{md} \tag{11}$$

Where A_{ed} and A_{md} stand for electric dipole and magnetic dipole respectively and both are calculated using equation (9) and (10) respectively:

$$A_{md} = \frac{64\,\pi^4 v^3}{3h\,(2J+1))}(\chi_{md} S_{md}) \tag{12}$$

$$A_{md} = \frac{64\,\pi^4 v^3}{3h\,(2J+1))}(\chi_{md} S_{md}) \tag{13}$$

χ_{ed} and χ_{md} **is** for the local – field correction for electric dipole and magnetic dipole transition, respectively**.** Both are obtained by using the ralations**:**

$$\chi_{ed} = \frac{n(n^2+2)^2}{9} \tag{14}$$

$$\chi_{md} = n^3 \tag{15}$$

The line-strength for magnetic dipole and electric dipole transition represented by S_{md}, S_{ed} , respectively. Both are given by the relations:

$$S_{md}(aJ, bJ') = \frac{e^2}{4m^2c^2}|< aJ|L + 2S|bJ' >|^2 \tag{16}$$

$$S_{ed}(aJ, bJ') = e^2 \sum_{\lambda=2,4,6} \Omega_\lambda |< aJ|U^{(\lambda)}|bJ' >|^2 \tag{17}$$

From the table 5, the $^4I_{15/2} \rightarrow {}^2H_{11/2}$ and $^4I_{15/2} \rightarrow {}^4F_{7/2}$ transition have high values for A_R. In addition, these $^2H_{11/2}$ and $^4F_{7/2}$ increase in A_R values when concentration of vanadium increase in the glass samples. It indicates the transition of $^2H_{11/2}$ and $^4F_{7/2}$ are beneficial to green and blue emission suitable for laser, respectively [38].

Preprints (www.preprints.org) | NOT PEER-REVIEWED | Posted: 9 March 2021 doi:10.20944/preprints202103.0259.v1

In addition, the radiative lifetime is very important data for laser and optical amplifier. The radiative lifetime (τ_{rad}) of prepared glass is a reciprocal of the total transition probabilities of an emission state $\sum_{bJ'} A(aJ, bJ')$ (sum of transition probabilities of all the transition from highest state to various lower states):

$$\tau_{rad} = \frac{1}{\sum_{bJ'} A(aJ,bJ')} \quad (18)$$

Lastly, the emission branching ratio are given by relations,

$$\beta_R(aJ, aJ') = \frac{A_R(aJ,bJ')}{\sum_{bJ'} A_R(aJ,bJ')} \quad (19)$$

The obtained values of τ and β_R are listed in table 5. The probability of simulated emission acquisition can be determined by the values of branching ratio for a specific transition [42]42]. The values or branching ration for transition of $^4I_{15/2} \rightarrow {}^2H_{11/2}$ and $^4I_{15/2} \rightarrow {}^4F_{7/2}$ is 99 % and the value of radiative ratio in the range 0.007151 - 0.004662. the value of the present glass is shorter compared to other glass system. The shorter radiative lifetime of this transition was beneficial for the control of the strong emission of erbium ion within the prepared glass system and the suppression of the non-radiative process.

Table 5. This is a table for values of A_R (s^{-1}), β_R (%), and τ (ms) of all prepared glass samples.

Trans.	**Para.**	***x* = 0 mol%**	***x* = 0.5 mol%**	***x* = 1.0 mol%**	***x* = 1.5 mol%**	***x* = 2.0 mol%**	***x* = 2.5 mol%**
$^4I_{15/2} \rightarrow$ $^4I_{11/2}$	A (s^{-1})	350.4501	345.0766	342.6103	399.3329	402.1335	510.5991
	β_R (%)	88.28409	87.94597	86.73962	87.97895	88.03274	86.71063
	τ (ms)	0.285347	0.289791	0.291877	0.250418	0.248674	0.195848
$^4I_{15/2} \rightarrow$ $^4I_{9/2}$	A (s^{-1})	388.3049	417.4752	421.7802	446.074	466.7488	585.5573
	β_R (%)	89.35107	89.29065	89.17369	89.32156	89.36282	89.19673
	τ (ms)	0.25753	0.239535	0.23709	0.224178	0.214248	0.170777
$^4I_{15/2} \rightarrow$ $^4F_{9/2}$	A (s^{-1})	3528.567	3702.558	3723.815	3982.301	4127.788	5193.279
	β_R (%)	80.94964	80.95793	80.89709	80.92708	80.87394	80.79215
	τ (ms)	0.02834	0.027008	0.026854	0.025111	0.024226	0.019256
$^4I_{15/2} \rightarrow$ $^4S_{3/2}$	A (s^{-1})	1104.706	1069.927	1066.042	1198.596	1229.809	1561.382
	β_R (%)	71.19585	71.16164	71.07426	71.14514	71.1602	71.06043
	τ (ms)	0.090522	0.093464	0.093805	0.083431	0.081313	0.064046
$^4I_{15/2} \rightarrow$ $^2H_{11/2}$	A (s^{-1})	14239.16	14798.61	13983.96	18283.85	17738.21	21451.45
	β_R (%)	99.18245	99.19011	99.0167	99.24465	99.22142	99.04161
	τ (ms)	0.007023	0.006757	0.007151	0.005469	0.005638	0.004662
$^4I_{15/2} \rightarrow$ $^4F_{7/2}$	A (s^{-1})	4326.441	4339.731	4338.381	4773.069	4928.462	6225.356
	β_R (%)	99.92411	99.9221	99.9106	99.91839	99.92096	99.90685
	τ (ms)	0.023114	0.023043	0.02305	0.020951	0.02029	0.016063

3.6 Photoluminescence

Preprints (www.preprints.org) | NOT PEER-REVIEWED | Posted: 9 March 2021 doi:10.20944/preprints202103.0259.v1

Figure 10 reveals the photoluminescence (PL) emission spectra of the (59.5 - x) B_2O_3-20Na_2O-20CaO – xV_2O_5 – Er_2O_3 - 0.5AgCl (x = 0, 0.5, 1.0, 1.5, 2.0 and 2.5 mol%) glass samples in the wavelength range 400 – 800 nm. The excitation wavelength was 800 nm. The emission spectra of Er^{3+} ions exhibited three dominant peaks at 516 nm, 580 nm, and 673 nm. These peaks were assigned to $^2H_{11/2}$ – $^4I_{15/2}$, $^4S_{3/2}$ – $^4I_{15/2}$, and $^4F_{15/2}$ – $^4I_{15/2}$. The band at 516 nm, 580 nm, and 673 nm due to stark splitting effects. The stark splitting effect because of low symmetry of the local environment around erbium ion [44]. The intensity increases when the concentration of V_2O_5 increases from 0 mol% to 1.5 mol%. However, when the concentration of vanadium more than 1.5 mol%, the intensity decreases. Thus, the decrement was due to a concentration quenching [44, 45]. It is suggested that, at a higher amount of vanadium, the excess vanadium ions produce structural defects that cause non-radiative recombination process. The transition from excited state to the visible wavelength can be ascribed by the emission of peaks at 516nm, 580nm, and 673nm [44].

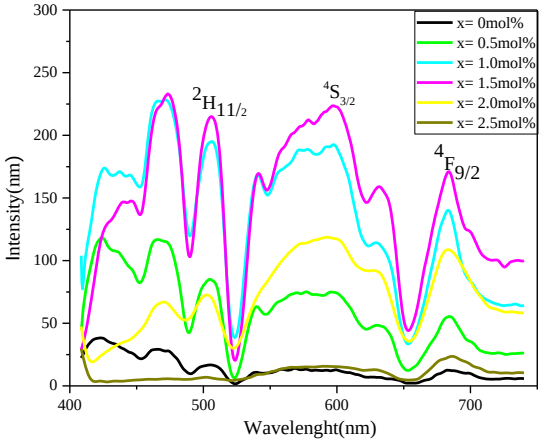

Figure 10. This is a figure of emission spectra of all the glass samples with excitation wavelength at 800 nm.

4. Conclusions

The effect of V_2O_5 substitution on structural and optical properties (59.5 – x) B_2O_3 – 20Na_2O – 20CaO – xV_2O_5 – Er_2O_3 – 0.5AgCl (x = 0, 0.5, 1.0, 1.5, 2.0 and 2.5 mol%) glasses were investigated. The glass had been successfully prepared via the melt-quenching method. The structural of the samples by XRD has indicated the glasses have amorphous nature without any crystalline phase when addition of vanadium. Meanwhile, the FTIR revealed the structural units in the glasses network. Thus, the FTIR confirmed the presence of B-O-B starching in borate network, bending vibration from the V – O – V of the VO_4 tetrahedral group, vibration of the B – O – V bridging bond, and stretching vibration B – O bond belong to BO_3. Addition of vanadium more or equal to 1.0 mol% create more NBO in the glass structural. Vis-NIR spectra exhibit eight absorption band which are 490, 520, 540, 660, 800, and 980 nm. All the peaks are referring the erbium absorption from the ground state $^4I_{15/2}$ to the excited states $^4F_{7/2}$, $^2H_{11/2}$, $^4S_{3/2}$, $^4F_{9/2}$, $^41_{9/2}$, and $^41_{11/2}$ respectively and the most intense peak centered at 540 nm and called as hypersensitive transition. The SPR band and vanadium band does not observe in the recorded spectra due to low concentration of silver nanoparticle and dominance of erbium band. The increase in vanadium is found to reduce band gap energy and increase the refractive index and Urbach energy from 2.359592 to 2.852138 and 0.298338 eV to 0.762137 eV. According to Judd – Ofelt principle, the spectroscopic parameter was calculated such as Judd – Ofelt parameter, quality factor, radiative lifetime, and branching ratio. The Judd – Oflet parameter was

revealed to follow the trend $\Omega_2 > \Omega_4 > \Omega_6$. The photoluminescence spectra exhibit three band at 516 nm, 580 nm, and 673 nm which are represented by $^2H_{11/2} - {}^4I_{15/2}$, $^4S_{3/2} - {}^4I_{15/2}$, and $^4F_{15/2} - {}^4I_{15/2}$, respectively. The obtained results of Judd – Ofelt and photoluminescence shows the glass samples with 1.0 mol% of vanadium is very useful in green laser application since have high values of lifetime, branching ratio and strong spectral intensity compare to other samples.

5. Patents

Author Contributions: N.A.Z and S.N.M completed the data collection. N.A.Z as a first author drafted the first manuscript. Z.M revised the manuscript and have approved the final of the manuscript for publication.

Funding: This research was funded by the Higher Education Malaysia under fundamental research grant scheme, 600 – IRMI/FRGS 5/3 (038/2019).

Acknowledgments: The author would like to express gratitude to Research Management Centre, Universiti Teknologi Mara for assistance throughout the research.

Conflicts of Interest: The authors declare no conflict of interest.

References

1. K. Selvaraju and K. Marimuthu, "Structural and spectroscopic studies on concentration dependent $Er^{3þ}$ doped boro – tellurite glasses," J. Lumin., 2012, 132, 1171 – 1178.
2. R. De Almeida, M. Davinson, and L. R. P. Kassab, "Eu^{3+} luminescence in tellurite glasses with gold nanostructures." Optics Communication, 2012, 218, 108 – 112
3. S. Rani, S. Sanghi, N. Ahlawat, and A. Agarwal, "Influence of Bi_2O_3 on thermal, structural and dielectric properties of lithium zinc bismuth borate glasses," J. Alloys Compd., 2014, 597, 110 – 118.
4. P. Pascuta, G. Borodi, and E. Culea, "Influence of europium ions on structure and crystallization properties of bismuth borate glasses and glass ceramics," J. Non. Cryst. Solids, 2008, 354, 5475 – 5479.
5. S. N. Mohamed and A. K. Yahya, "Effects of V_2O_5 on elastic, structural, and optical properties of mixed ionic – electronic $20Na_2O - 20CaO - (60 - x)\ B_2O_3 - xV_2O_5$ glasses," Ionics (Kiel)., 2017, 1 – 18.
6. N. Syahidah, A. K. Yahya, R. Abd – Shukor, and M. Kumar, "Anomalous elastic behaviour of $xSrO - 10PbO - (90 - x)\ B_2O_3$ glass system," J. Non. Cryst. Solids, 2016, 444, 55 – 63.
7. S. Kabi and A. Ghosh, "Mixed glass former effect in AgI doped silver borophosphate glasses," Solid State Ionics, 2013, 90, 3 – 6.
8. C. Narayana, "Electronic and ionic conductivity studies on microwave synthesized glasses containing," Integr. Med. Res., 2016, 205, 2 – 7.
9. M. Saad, W. Stambouli, S. A. Mohamed, and H. Elhouichet, "Ag nanoparticles induced luminescence enhancement of Eu^{3+} doped phosphate glasses Moufida," J. Alloys Compd., 2016, 2017, 1 – 29.
10. K. M. Kaky, G. Lakshminarayana, S.O. Baki, A. Lira, U. Caldi , A.N. Meza-Rocha, C. Falcony, I.V. Kityk, Y.H. Taufiq-Yap, M.K. Halimah, and M.A. Mahdi, "Structural and optical studies of $Er^{3þ}$ – doped alkali / alkaline oxide containing zinc boro – aluminosilicate glasses for 1.5 mm optical amplifier applications," Optical Materials, 2017, 69, 401 – 419.
11. K. Neeraja, T. G. V. M. Rao, A. R. Kumar, N. Veeraiah, and M. R. Reddy, "Influence of modifier oxide on Spectroscopic properties of Ho^{3+}: V^{4+} co – doped $Na_2O - SiO_2 - ZrO_2$ glasses," Alloy. Compd., 2014, 586, 159 – 168.
12. G. Tang, X. Wen, Q. Qian, T. Zhu, and W. Liu, "Efficient 2.0 mm emission in $Er^{3þ}/Ho^{3þ}$ co – doped barium gallo – germanate glasses under different excitations for mid-infrared laser," J. Alloys Compd., 2016, 664, 19 – 24.
13. K. Neeraja, T. G. V. M. Rao, A. R. Kumar, V. U. Lakshmi, N. Veeraiah, and M. R. Reddy, "Spectroscopic properties of Sm^{3+} and V^{4+} ions in $Na_2O - SiO_2 - ZrO_2$ glasses," Mol. Struct., 2013, 1055, 339 – 348.
14. A. S. Alqarni, R. Hussin, S. K. Ghoshal, S. N. Alamri, Y. A. Yamusa, and S. A. Jupri, "Intense red and green luminescence from holmium activated zinc – sulfo – boro – phosphate glass: Judd – Ofelt evaluation," J. Alloys Compd., 2019, 808, 151706.
15. M. S. Gaafar, N. S. A. El-Aal, O. W. Gerges, and G. El-Amir, "Elastic properties and structural studies on some zinc – borate glasses derived from ultrasonic, FT– IR and X – ray techniques," J. Alloys Compd., 2009, 475, 535 – 542.
16. A. Awang, S. K. Ghoshal, M. R. Sahar, M. Reza Dousti, R. J. Amjad, and F. Nawaz, "Enhanced spectroscopic properties and Judd – Ofelt parameters of Er – doped tellurite glass: Effect of gold nanoparticles," Curr. Appl. Phys., 2013, 13, no. 8, 1813 – 1818.
17. M. Farouk, A. Samir, F. Metawe, and M. Elokr, "Optical absorption and structural studies of bismuth borate glasses containing Er^{3+} ions," J. Non. Cryst. Solids, 2013, 371 – 372, 14 – 21.
18. M. S. Gaafar, Y. B. Saddeek, and L. Abd El-Latif, "Ultrasonic studies on alkali borate tungstate glasses," J. Phys. Chem. Solids, 2009, 70, 173 – 179.

19. V. Kundu, R. L. Dhiman, A. S. Maan, and D. R. Goyal, "Structural and Physical Properties of Fe_2O_3 – B_2O_3 – V_2O_5 Glasses," Adv. Condens. Matter Phys., 2008, 2008, 1 – 7.
20. G. Broglia, C. Mugoni, J. Du, C. Siligardi, and M. Montorsi, "Lithium vanado – phosphate glasses: Structure and dynamics properties studied by molecular dynamics simulations," J. Non. Cryst. Solids, 2014, 403, 53 – 61.
21. S. K. Arya, G. Kaur, and K. Singh, "Effect of vanadium on the optical and physical properties of lithium borate glasses," J. Non. Cryst. Solids, 2015, 432, 3 – 8.
22. F. H. Margha, M. A. Marzouk, "Influence of vanadium addition on the optical and photoluminescence properties of borate glasses and their glass – ceramic derivatives," Appl. Phys. 2019, 5, 1 – 9.
23. A. M. Abdelghany and A. H. Hammad, "Impact of vanadium ions in barium borate glass," Spectrochim. Acta – Part A Mol. Biomol. Spectrosc., 2015, 137, 39 – 44.
24. R. J. Amjad, M. R. Dousti, and M. R. Sahar, "Spectroscopic investigation and Judd – Ofelt analysis of silver nanoparticles embedded Er^{3+}– doped tellurite glass," Curr. Appl. Phys., 2015, 15, 1 – 7.
25. Z. Jiang, G. Wen, Y. Luo, X. Zhang, Q. Liu, and A. Liang, "A new silver nanorod SPR probe for detection of trace benzoyl peroxide," Sci. Rep., 2014, 4, 1 – 6.
26. R. Rajaramakrishna, S. Karuthedath, R. V. Anavekar, and H. Jain, "Nonlinear optical studies of lead lanthanum borate glass doped with Au nanoparticles," J. Non. Cryst. Solids, 2012, 358, 1667 – 1672.
27. M. Reza Dousti and R. J. Amjad, "Effect of silver nanoparticles on the upconversion and near – infrared emissions of Er^{3+}: Yb^{3+} co – doped zinc tellurite glasses," Meas. J. Int. Meas. Confed., 2017, 105, 114 – 119.
28. M. F. Maulud and A. K. Yahya, "Influence of germanate anomaly on elastic, structural, and optical properties lead – germanate glasses," Mater. Res., 2016, 357, 1 – 11.
29. G. S. Opelt, "Intensities of crystal spectra of rare – earth ions," J. Chem. Phys., 1962, 37, 511 – 520.
30. B. R. Judd, "Optical absorption intensities of rare – earth ions," Phys. Rev., 1962, 127, 750 – 761.
31. A. Maaoui, M. Haouari, Z. Zaaboub, I. Fraj, F. Saidi, and H. Ben Ouada, "Concentration effects on the optical spectroscopic properties of Er^{3+} – doped TeO_2 – Nb_2O_5 – ZnO vitreous system," J. Alloys Compd., 2016, 663, 395 – 406.
32. N. Abdedou, T. Djouama, M. Chalal, M. Poulain, B. Capoen, and R. Mahiou, "Synthesis and characterization of Er^{3+}/Cu^{+} – codoped fluorophosphate glasses," J. Alloys Compd., 2019, 790, 248 – 256.
33. N. N. Yusof, S. K. Ghoshal, and M. N. Azlan, "Optical Properties of Titania Nanoparticles Embedded Er^{3+}– Doped Tellurite Glass: Judd – Ofelt Analysis," J. Alloys Compd., 2017, 724, 1 – 22.
34. J. Rajagukguk, Fitrilawati, B. Sinaga, and J. Kaewkhao, "Structural and spectroscopic properties of Er^{3+} doped sodium lithium borate glasses," Spectrochim. Acta – Part A Mol. Biomol. Spectrosc., 2019, 223, 117342.
35. N.Vijayaa, P.Babu, V.Venkatramu, C.K.Jayasankara, S.F.León-Luis, U.R.Rodríguez-Mendozad, I.R.Martínd, V.Lavínd, "Optical characterization of Er^{3+}– doped zinc fluorophosphate glasses for optical temperature sensors," Sensors Actuators, B Chem., 2013, 186, 156 – 164.
36. S. F. León-Luis, U. R. Rodríguez-Mendoza, P. Haro-González, I. R. Martín, and V. Lavín, "Role of the host matrix on the thermal sensitivity of Er^{3+} luminescence in optical temperature sensors," Sensors Actuators, B Chem., 2012, 174, 176 – 186.
37. S. B. Rice, C. Chan, S. C. Brown, P. Eschbach, L. Han, D. S. Ensor, A. B. Stefaniak, J. Bonevich, A. E. Vladár, A. R. H. Walker, J. Zheng, C. Starnes, A. Stromberg, J. Ye and E. A. Grulke, "Particle size distributions by transmission electron microscopy: An interlaboratory comparison case study," Metrologia, 2013, 50, 663 – 678.
38. A. M. Noorazlan, H. M. Kamari, S. O. Baki, and D. W. Mohamad, "Green Emission of Tellurite Based Glass Containing Erbium Oxide Nanoparticles," 2017, 724, 1083 – 1092.
39. A. Miguel, J. Azkargorta, R. Morea, I. Iparraguirre, J. Gonzalo, J. Fernandez, and R. Balda, "Spectral study of the stimulated emission of Nd^{3+} in fluorotellurite bulk glass," Opt. Express, 2013, 21, 9298.
40. I. Jlassi, H. Elhouichet, S. Hraiech, and M. Ferid, "Effect of heat treatment on the structural and optical properties of tellurite glasses doped erbium," J. Lumin., 2012, 132, 832 – 840.
41. I. A. Rayappan and K. Marimuthu, "Structural and luminescence behavior of the Er^{3+} doped alkali fluoroborate glasses," J. Non. Cryst. Solids, 2013, 367, 43 – 50.
42. D. K. Sardar, J. B. Gruber, B. Zandi, J. A. Hutchinson, and C. Ward Trussell, "Judd – Ofelt analysis of the $Er^{3+}(^4F_{11})$ absorption intensities in phosphate glass: Er^{3+}, Yb^{3+}," J. Appl. Phys., 2003, 93, 2041 – 2046.
43. I. Jlassi, H. Elhouichet, M. Ferid, and C. Barthou, "Judd – Ofelt analysis and improvement of thermal and optical properties of tellurite glasses by adding P_2O_5," J. Lumin., 2010, 130, 2394 – 2401.
44. W. D. Pyrz and D. J. Buttrey, "Particle size determination using TEM: A discussion of image acquisition and analysis for the novice microscopist," Langmuir, 2008, 24, 11350 – 11360.
45. H. N. Baig, J. K. Saluja, and S. J. Dhoble, "Synthesis and characterization of erbium – doped $YAlO_3$ phosphor," Luminescence, 2016, 31, 401 – 406.
46. O. Olvera-R, K. Chamé-F, J. J. Sánchez-Mondragón, M. T. Cisneros, M. L. Ojeda, and C. Velásquez, "Effect of the trivalent erbium concentration on the luminescent properties of TiO2 Er^{3+} composites," Comput. y Sist., 2019, 23, 89 – 94.